New Astronomy 15 (2010) 8–15

Contents lists available at ScienceDirect

New Astronomy

journal homepage: www.elsevier.com/locate/newast

Signature of slow acoustic oscillations in a non-flaring loop observed by EIS/Hinode

A.K. Srivastava [a], B.N. Dwivedi [b,*]

[a] Aryabhatta Research Institute of Observational Sciences (ARIES), Nainital 263129, India
[b] Department of Applied Physics, Institute of Technology, Banaras, Hindu University, Varanasi 221005, India

ARTICLE INFO

Article history:
Received 5 July 2008
Received in revised form 17 April 2009
Accepted 12 May 2009
Available online xxxx

PACS:
96.60.–j

Keywords:
Corona
Corona loops
MHD waves
Oscillations

ABSTRACT

We study intensity oscillations near the apex of a coronal loop to find the signature of MHD oscillations. We analyse the time series of the strongest Fe XII 195.12 Å image data, observed by 40″ SLOT of the EUV Imaging Spectrometer (EIS) onboard the Hinode spacecraft. Using a standard wavelet tool, we produce power spectra of intensity oscillations at location 'L_3' near the apex of a clearly visible coronal loop. We detect intensity oscillations of a period of ≈322 s with a probability of 96%. This oscillation period of ≈322 s is found to be in good agreement with theory of the multiple (first and second) harmonics of standing slow acoustic oscillations of $P_{2nd\,slow} \approx 313 \pm 31$ s. We detect, for the first time, the observational signature of multiple (first and second) harmonics of slow acoustic oscillations in the non-flaring coronal loop. Such oscillations have been observed in the past in hot and flaring coronal loops only, but have been predicted recently to exist in comparatively cooler and non-flaring coronal loops as well. We find the periodicities ∼497 s and ∼592 s with the probability 99–100% at the 'L_1' and 'L_2' locations, respectively, near the clearly visible western footpoint of the loop. We interpret these oscillations to be likely associated with the first harmonics (fundamental mode) of slow acoustic oscillations. Using the period ratios $P_1/P_2 = 1.54$ and 1.84, we estimate the density scale heights in the EUV loop as ∼10 Mm and 21 Mm, respectively, in which the latter value (∼21 Mm) is compared well with the loop half length. We also find an evidence of propagating bright blob at its lower bound sub-sonic speed of ≈6.4 km/s, suggesting that they are caused by the mass flow from one end to the other in the coronal loop. We also suggest that standing oscillations, and propagating bright blobs caused probably by the pulse of plasma flow, co-exist in comparatively cooler and non-flaring coronal loop.

1. Introduction

The mega-Kelvin hot solar plasma, embedded in a complex magnetic field, is a cosmic laboratory that we are best able to observe with the possible exception of the Earth's magnetosphere system, for the generation of a variety of magnetohydrodynamic (MHD) waves and oscillations. Study of these waves and oscillations provides important clues to understanding the physics of the solar corona, its heating and the solar wind acceleration mechanisms. Magnetically structured coronal loops, anchored into the photosphere, exhibit various kinds of MHD oscillations, such as fast sausage, kink, slow acoustic oscillations, etc. The idea of exploiting such observed oscillations as a diagnostic tool for deducing physical parameters of coronal plasma was first suggested by Roberts et al. (1984). This has been investigated extensively analyzing data from space (e.g., Nakariakov et al., 1999; Aschwanden et al., 1999a; Nakariakov and Ofman, 2001). However, the real progress on this 'hot topic' was made with the availability of high-resolution observations from space (e.g., SoHO and TRACE) and most recently with the high-resolution spectra and images from the instruments onboard the Hinode spacecraft.

There exist many observed MHD oscillation modes in various coronal structures. The fast kink waves have been detected by the periodic spatial displacement of coronal loop axis (Nakariakov et al., 1999; Aschwanden et al., 1999a; Wang and Solanki, 2004). The simultaneous existence of fundamental (or first) and second harmonics of fast kink oscillations have also been reported (e.g., Verwichte et al., 2004; Van Doorsselaere et al., 2007). De Moortel and Brady (2007) interpreted the observed oscillations as co-existence of 2nd and 4th harmonics of fast kink oscillations. O'Shea et al. (2007) have found the first evidence of different harmonics of fast kink standing oscillations in cool transition region loops. The fast sausage MHD oscillations cause the variation of pressure and magnetic field in the coronal loop, which can be observed as an intensity oscillation or periodic modulation of coronal radio emissions (Aschwanden, 1987; Nakariakov et al., 2003). Recently, Srivastava et al. (2008a) have found the first signature of long-period multiple sausage oscillations in cool post flare loops, and suggested that such oscillations can be possible only in highly overdense cool post flare loops.

* Corresponding author. Tel.: +91 542 2307041.
E-mail address: bholadwivedi@gmail.com (B.N. Dwivedi).

1384-1076/$ - see front matter © 2009 Elsevier B.V. All rights reserved.
doi:10.1016/j.newast.2009.05.006

While fast kink and sausage oscillations are commonly detected in different types of solar loops, standing slow acoustic oscillations have been observed in hot and flaring coronal loops only. Strongly damped Doppler shift oscillations in hot ($T > 6.0$ MK) and flaring loops have been observed with SoHO/SUMER (Wang et al., 2002, 2005). These oscillations are interpreted as fundamental mode standing slow acoustic waves (Ofman and Wang, 2002) and are excited by impulsive energy releases, localised near loop footpoints, at a frequency corresponding to the fundamental mode frequency (Taroyan et al., 2005). Nakariakov et al. (2004) and Tsiklauri et al. (2004) have suggested that oscillations with periods of 10–300 s in hot and flaring coronal loops may be due to the standing slow acoustic wave, which is excited by impulsive energy releases localised in the corona. However, standing slow acoustic oscillations have remained undetected in cooler, non-flaring coronal loops, although there is plenty of evidence for propagating slow acoustic waves in these loops (e.g., Robbrecht et al., 2001; De Moortel et al., 2000, 2002; Sakurai et al., 2002; King et al., 2003). One reason for this could be that propagating acoustic waves are driven by the penetration into the corona of sub-photospheric p-modes, although Taroyan and Bradshaw (2008) show that propagating acoustic waves can also be driven by impulsive energy releases, localised near loop footpoints, at frequencies differing from the fundamental mode frequency.

In view of the fact that the observations of slow acoustic standing oscillations offer a unique opportunity to understanding the coronal plasma, the lack of evidence of similar oscillations and the understanding of exact excitation/damping mechanisms in cooler loops remained a puzzle. Using 1-D hydrodynamic loop model, Taroyan and Bradshaw (2008) simulated the observables of the various harmonics of slow acoustic oscillations in EIS, but did not specially discuss excitations of the second harmonic. They predicted that various harmonics of slow acoustic oscillations can also be observed from EIS/Hinode real observations of cooler and non-flaring coronal loops, using spectral as well as temporal image data. Using spectroscopic observations from EIS/Hinode 1″ slit, Erdélyi and Taroyan (2008) have recently reported first observational signature of slow acoustic oscillations in the cooler non-flaring loops. In this paper, we report the first signature of the multiple harmonics of slow acoustic oscillations in non-flaring coronal loops, using temporal image data from EIS/Hinode 40″ slot. We study the spectrum of intensity oscillations near the apex as well as footpoint of the coronal loop, using new data acquired from EIS/Hinode. We analyse the observational results in terms of different MHD modes, and interpret them as the multiple (first and second) harmonics of slow acoustic oscillations. We also find an evidence of co-existence of propagating bright blob at its lower bound sub-sonic speed of ≈6.4 km/s, suggesting that they are caused by pulse of plasma flow.

In Section 2, we present observations and data reduction. We describe wavelet analysis and randomisation techniques in Section 3. In Section 4, we present a theoretical interpretation. The discussion and conclusions are given in the last section.

2. Observations and data reduction

We use time series data of the on-disk active region loops as observed by the 40″-slot of EIS (Culhane et al., 2006). The 40″ and 266″ slots are appropriate for image analyses using light curves, while 1″ and 2″ slits are ideal for spectral and Doppler analyses using spectral line profiles. EIS observes high resolution spectra in two wavelength intervals 170–211 Å and 246–292 Å, by short-wavelength (SW) and long-wavelength (LW) CCDs, respectively. The spectral resolution of EIS is 0.0223 Å per pixel. There are approximately 16–20 pixels and ∼2 pixels offsets, in the Y and X-coordinates, respectively of two CCDs (Young et al., 2007). Observations were acquired on 8 May 2008, and the name of this study is StA_loop_slot_lo. The data contains Fe XI 188.23 Å, Fe XII 195.12 Å, Fe XIII 202.04, 203.83 Å, Fe XIV 274.2 Å, Fe XV 284.12 Å, Fe XVI 262.92 Å, and Ca XVII 192.82 Å EUV lines. The observation started at 09:35:20 U.T., and ended at 10:10:49 U.T. The position of the X-centre and Y-centre of the slot, were 245.04″ and −399.84″, respectively, while the X-FOV and Y-FOV, were 40″ and 248″, respectively (Fig. 1). The binning of the data was 1″ × 1″. The observation window on the CCDs is with a height of 248 pixels along the SLOT and a width of 40 pixels in the wavelength direction. The exposure time for the observations was 20 s, and the integration time for each step of the time series was uniform, being 20 s.

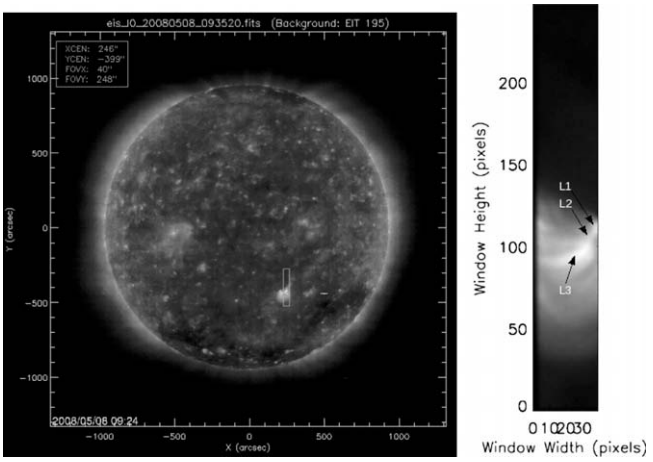

Fig. 1. The pointing position of 40″ slot over the full disk image of SoHO/EIT (left), and the brightened coronal loop system is shown in Fe XII 195.12 Å line (right). The position on the full disc image is expressed in arc sec and the position on the slot in pixels. Three locations L_1, and L_2 (near loop footpoint), and L_3 (near loop apex) have been shown from where the EUV light curves are derived for the power spectrum analyses.

We apply standard EIS data-reduction procedures, to the data acquired at the telescope (the raw (zeroth level) data). The subroutines can be found in the SSWIDL software tree.[1] These standard subroutines correct for dark-current subtraction, cosmic-ray removal, flat-field correction, hot pixels, warm pixels, and bad/missing pixels. The data is saved in the level-1 data file, while associated errors are saved in the error file. Since we are analyzing the cooler coronal loops formed around 1.58 MK in the inner corona, we do not include time-series image data from high temperature coronal lines, e.g., Fe XIV, XV, XVI, and Ca XVII. Moreover, the power spectrum analysis needs the light curves with good and enough signal-to-noise (S/N) ratio, hence we have chosen Fe XII 195.12 Å strongest core line, to produce the power spectrum of its time series image data. We choose the location L_3 near the apex of a clearly visible loop $[(X_\lambda, Y_{SLOT}) = (28.28\text{th pixel}, 95.52\text{th pixel})]$, and the locations $L_1[(X_\lambda, Y_{SLOT}) \sim (37\text{th pixel}, 112\text{th pixel})]$ and $L_2[(X_\lambda, Y_{SLOT}) \sim (32\text{th pixel}, 103\text{th pixel})]$ near the western footpoint. We extract the light curves from the time-series image data of strongest EIS core line Fe XII 195.12 Å with strong S/N ratio enough for the statistical analyses. For example, the signal-to-noise ratios (S/N) of selected line (Fe XII 195.12 Å) is in the range of 104–115 for the time series extracted from near the loop apex, which is adequate for our study. The summation of X or Y pixels was not completed, to prevent information losses about coronal loops in the on-disk active region. We extract the nascent light curves from various locations inside the clearly visible loop near its apex as well as footpoint, and we do not perform

[1] e.g., http://www.darts.isas.jaxa.jp/pub/solar/ssw/hinode/eis/.

the background subtraction. We execute wavelet analysis of the extracted EUV light curves from the time series observed by 40″ slot. We find the statistically significant periodicities from the intensity wavelet spectra. Hence, the background subtraction with the nearby quiet region is not necessary for such analyses. However, the background subtraction is significant when we analyse the slit rasters or time series for plasma diagnostics, e.g., density, temperature, line width, Doppler velocity, etc. By fitting spectral lines observed from either 1″ or 2″ EIS-slit, we can only measure accurately the peak intensity, line width, and centroid of line after background subtraction. Hence, one should take account of such subtractions in spectral data analysis.

The EIS pointing associated with the observed data may have jitters in both X and Y directions up to several arcsec. Therefore, we have checked our temporal image data using cross correlation technique. The measured jitters in the images are of sub-arcsec (or sub-pixels) in nature. Therefore, the jitter is unlikely to be the cause of any oscillations measured. We have also computed the cross-correlation coefficient which has value ≈'−1' at zero time lag. The temporal image data can have the maximum correlation when the correlation coefficient will be either '+1' or '−1'. Hence, the cross-correlation test of our temporal image data confirms its suitability for the statistical analyses.

3. Wavelet analysis

We use "Randomlet" software which has certain advantage in searching the statistically significant real periodicities in light curves over periodograms and Fourier power spectra which are used extensively in the literature. Wavelet analysis computer code "Randomlet" has been developed by E. O'Shea in the IDL environment software. Using this code, we can find statistically significant and real periodicities in the time series data. This software executes "Randomization Test" to examine the existence of statistically significant real periodicities in the time series data, if any. The programme executes randomization test which is an additional feature along with the standard wavelet analysis code (Torrence and Compo, 1998). Using this technique, many important results have been published by analyzing approximately uniformally sampled data in the solar physics context (e.g. Banerjee et al., 2001; O'Shea et al., 2001; O'Shea et al., 2005; Ugarte-Urra et al., 2004; Popescu et al., 2005; Srivastava et al., 2008a,b; O'Shea and Doyle, 2009), in AGN context (Gupta et al., 2009), and in the stellar context (Pandey and Srivastava, 2009).

Using wavelet analysis, the search for periodicities in light curves is carried out by a time localized function which is continuous in both frequency and time. The wavelet used in this study is the Morlet function which is defined as

$$\psi_t(s) = \pi^{-1/4} \exp(i\omega t) \exp\left(\frac{-t^2}{2s^2}\right), \quad (1)$$

where t, s, ω and $\pi^{-1/4}$, respectively, are the time parameter, wavelet scale, the oscillation frequency parameter, and the normalization constant. The Morlet function shows the product of sine wave with Gaussian envelop. The Fourier period P is related to the wavelet scales in the Morlet function by the relation: $P = 1.03$ s. The wavelet is convolved with the time series to determine the contribution of the frequency to the time series, which matches the sinusoidal portion by varying the scale of the wavelet function. This method produces the power spectrum of the oscillations in different light curves. We note that the Morlet wavelet suffers from an "edge effect" that is typical for analyses of time series data. However, this effect is significant only in regions falling within a cone of influence (COI) which demarks where possible periods, too close to either the measurement interval or the maximum length of the time series, cannot be convincingly detected. The randomlet software executes measurements of the peak power in the global wavelet spectrum, which is the average peak power over time, and is equivalent to a smoothed Fourier power spectrum. The randomization technique compares the average values to peak powers evaluated for $n!$ equally-likely permutations of the time series data, assuming that n values of measured intensities are independent of n measured times, if no periodic signal is present. The proportion of permutations that provides a value greater or equal to the original peak power of the time series, will provide the probability without periodic component (p). The percentage probability of periodic components present in the data, will be $(1 - p) \times 100$. For real oscillations, the lowest acceptable probability is 95% in the measurements. We have calculated 200 permutations of the reliable estimation of p, and hence the probability of real oscillations. The details of the randomisation technique used to examine the existence of statistically-significant real oscillation periods, have been given by Linnell Nemec and Nemec (1985) and O'Shea et al. (2001). We use the wavelet reconstruction method in order to find statistically significant real oscillation periods from below the COI region. The wavelet reconstruction method has also been used successfully in searching of fast oscillations in the magnetically active stars (Mathioudakis et al., 2006). Our time series data is dominant with the powers associated with the longer periods above the COI period. Therefore, we have chosen this method to find the statistically significant periods below the COI. The details of the wavelet reconstruction method is given in Mathioudakis et al. (2006) and Torrence and Compo (1998). The wavelet analysis of the Fe XII 195.12 Å EUV light curve derived near the loop apex $(X_\lambda, Y_{SLOT}) \sim$ (28th pixel, 95th pixel) is presented in Fig. 2. The time series was reconstructed over all scale values corresponding to the periods less than a period ∼600 s, which is below the COI period. The maximum allowed period from COI, where the edge effect is more effective, is 762 s. The intensity wavelet transform of our Fe XII 195.12 Å time series is shown in the middle-left panel of Fig. 2, where the darkest regions show the enhanced oscillatory power. The cross-hatched area is the cone of influence (COI), which is defined as the region of the power spectrum where edge effect may become effective due to the finite size of the time series. Hence, the power reduces substantially beyond this threshold. In our wavelet analysis, we consider only the power peaks and corresponding real periods below this threshold. The extent of the COI at each period is the decorrelation time of the wavelet function. This is equal to $\sqrt{2}P$ for the Morlet wavelet function, where P is the oscillatory period. Our choice of the cut-off period (∼600 s) for the filtering was based on the value of COI period (∼762 s) as the longer periods cannot exist for a decorrelation duration outside the COI. The middle right panel shows the global power spectrum of the time series. We measured periodicity of ∼322 s, with a probability of 96% in the time series of Fe XII 195.12 Å. These oscillations are most likely signature of the second harmonics of slow acoustic oscillations, while the relative intensity variation in the light curve is ∼12%. Finally, the bottom-left panel shows the probabilities of the presence of two specific frequencies (or periods) corresponding to the first and second highest powers shown in the middle-left panels as functions of the time after the start of the observations. The solid line represents the probability corresponding to the major power peak of time series data, while the dotted line corresponds to the secondary power peak. It should be also noted that both the periods show the probability 96% and 99–100%, respectively, as quoted in the right-bottom. However, we only consider the period corresponding to the first major power peak in our analysis as it is globally distributed in the intensity wavelet. It is clear from Fig. 2 that the first period near ∼322 s dominates between 15 and 35 min in the intensity wavelet of the time series outside the COI. Hence, there is at least the presence of ∼4 cycles of such oscillations in the time-series, which is statistically significant and treated as a

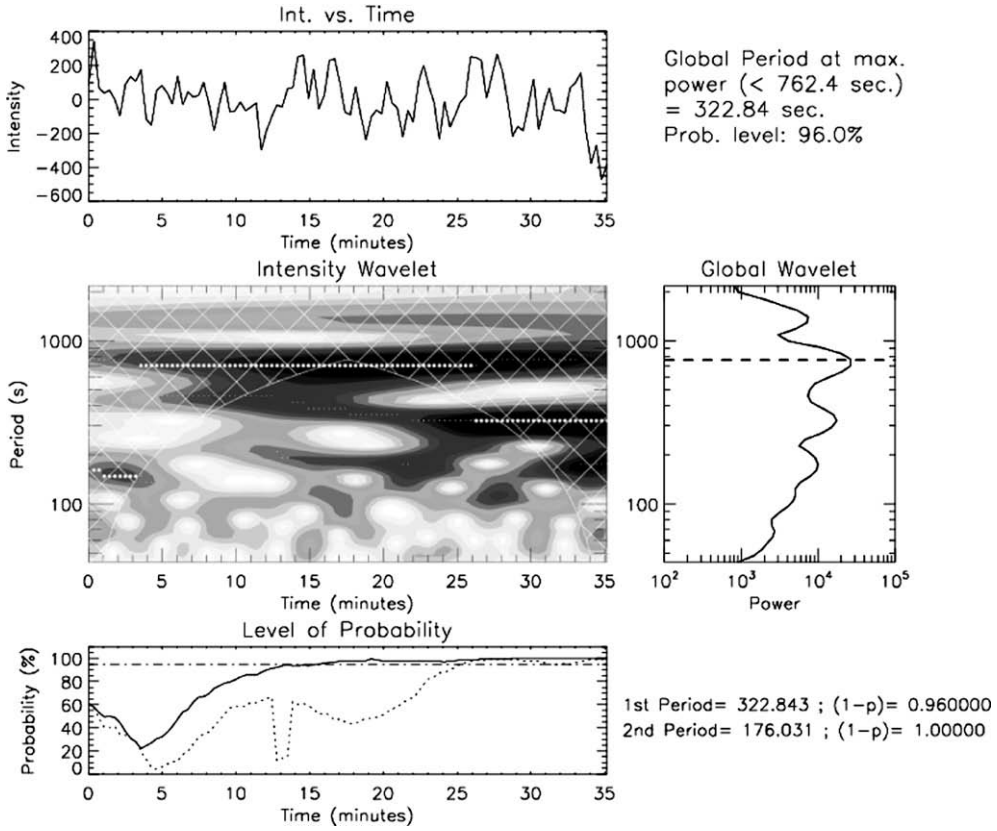

Fig. 2. The wavelet result for time series of Fe XII 195.12 Å: Top panel shows the variation of intensity, the wavelet power spectrum is given in the middle panel, and probability in the bottom panel. The light curve is extracted from L_3 location $(X_\lambda, Y_{SLOT}) \sim (28\text{th pixel}, 95\text{th pixel})$ near the loop apex.

global periodicity in the time series data with the probability of ~96%. However, the second period near ~176 s only dominates for very short time scales locally in the intensity wavelet spectrum, hence, cannot be considered as statistically significant global periodicity. Similarly, the period near ~760 s just lies in the COI region, hence we cannot consider it as a statistically significant period. We also derive our wavelet results by summing few pixels across within the selected loop. We have done summation of a few *y*-pixels, e.g., 3-pixels (~3 arcsec), and 4-pixels (~4 arcsec) across inside the selected loop to improve the signal-to-noise (S/N) ratio. For the former case, we get the same periodicity ~322 s with the probability of 98.5%, while for the latter case, we get the same periodicity ~322 s with the probability of 99.5%. Hence, our results confirm the presence of statistically significant and dominating oscillation period of ~322 s in the temporal image data from near the loop apex.

We derive the wavelet power spectrum of the EUV light-curve extracted from the L_1 location for the western footpoint of the loop $[(X_\lambda, Y_{SLOT}) \sim (37.056\text{th pixel}, 112.525\text{th pixel})]$, which shows the statistically significant periodicity of ~497 s with a probability of ~99–100%. This periodicity dominates the repetition of ~4 cycles over the total life span of the oscillation in the intensity wavelet of the time series outside the COI (cf., Fig. 3). Since the loop system is very complex and diffused, hence we choose another location L_2 also for the western footpoint $[(X_\lambda, Y_{SLOT}) \sim (32\text{th pixel}, 103\text{th pixel})]$ to extract the EUV light curve (relative intensity variation is ~5%) for the wavelet analysis, and obtain the power spectrum as shown in Fig. 4. We obtain the statistically significant periodicity of ~592 s with the probability of ~99–100%, and with the repetition of only ~2 cycles over the total life span of the oscillations. Our analyses except the one for L_2 location satisfy the recently reported more stringent criterion of O'Shea and Doyle (2009), i.e., at least the repetition of ~4 cycles over the total life span of the oscillations. Since such criterion is more strict but arbitrary in nature and the periodicity ~592 s which passes the randomization test with 99–100% probability cannot repeat even the 4 cycles over total span (35 min) of the time series, hence, we consider this periodicity as a statistically significant one. We also consider the periodicity ~497 s at location L_1 as a statistically significant one, because it is not only globally distributed (~4 cycles repetition) but also pass the randomization test (99–100% probability). Since the eastern footpoint is not fully exposed in the field of view, we do only consider the observed periodicity at western footpoint as the signature of first harmonics of the slow acoustic oscillations. We suggest the oscillations with period ~497 s or ~592 s may likely be associated with the first harmonics (or fundamental mode) of the slow acoustic oscillations at the western footpoint.

4. Theoretical interpretation

Measuring coronal loop length by assuming 10% uncertainty in the estimation of loop length (Nakariakov and Ofman, 2001), we find the loop length $L \approx (59.80 \pm 5.98)$ Mm. The loop is clearly not semi-circular but highly tilted (cf., Fig. 1, right panel). Therefore, we measured its half-length pixel-wise from the visible footpoint to its apex using the difference image in which loop strand is clearly visible. The total length is the twice of this length. We have taken the mean electron temperature and density as $T_e \approx 1.58$ MK (the formation temperature of Fe XII 195.12 Å in the inner corona), $n_e \approx 1.0 \times 10^9$ cm^{-3}. The period of second spatial harmonics of standing slow acoustic oscillations is (Tsiklauri et al., 2004):

$$P_{2nd\,slow} = \left(\frac{L}{c_s}\right) = \frac{L}{\left(1.52 \times 10^5 \sqrt{T}\right)} s, \qquad (2)$$

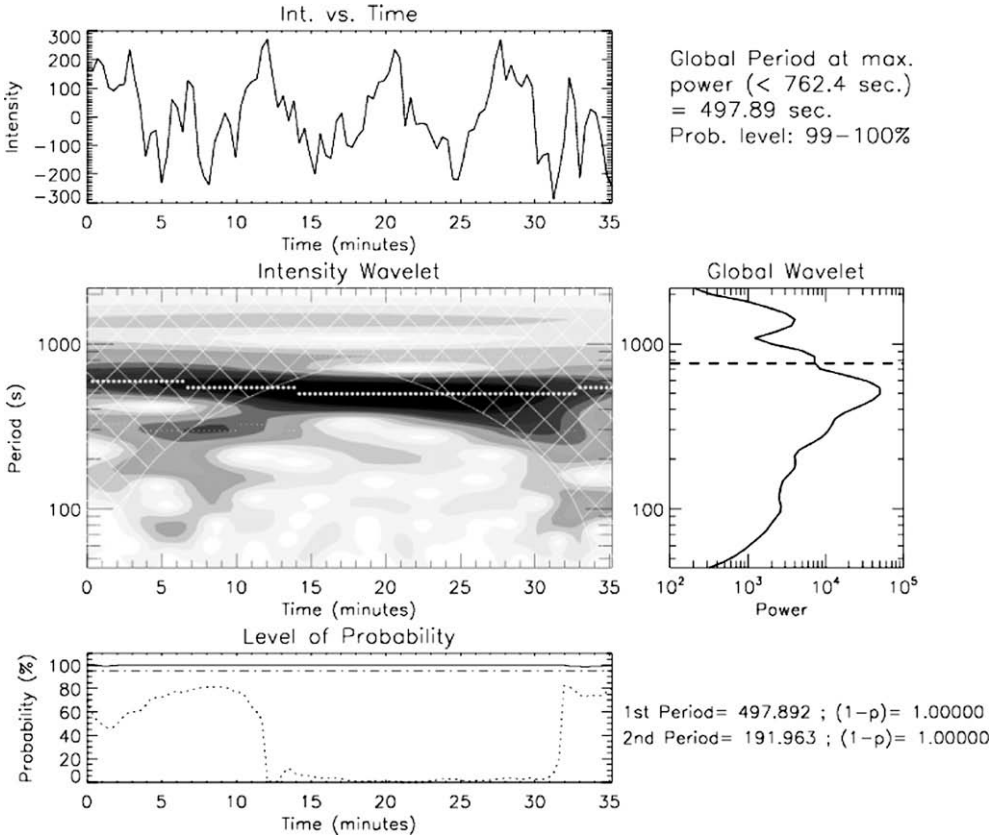

Fig. 3. The wavelet result for time series of Fe XII 195.12 Å: Top panel shows the variation of intensity, the wavelet power spectrum is given in the middle panel, and probability in the bottom panel. The light curve is extracted from L_1 location $(X_\lambda, Y_{SLOT}) \sim$ (37th pixel, 112th pixel) near the western footpoint.

where plasma temperature T is in MK, while loop length L is in meters. The period of first harmonic (or fundamental mode) must be double of the $P_{2^{nd}\,slow}$.

Using observationally estimated loop length, and adopting physical parameters for the inner corona, and Eq. (2), we estimate the period of $P_{2nd\,slow} \approx 313 \pm 31$ s for the second spatial harmonics of slow acoustic oscillations. The observationally derived oscillation period of ~322 s approximately matches with the theoretically derived oscillation period of the second harmonics of standing slow acoustic oscillations, i.e., $\approx 313 \pm 31$ s which provides the most likely signature of the second harmonics of slow acoustic oscillations in the loop.

Since formation temperatures of Fe IX, Fe X, Fe XI, and Fe XII overlap on each other in ionization equilibrium (cf., Arnaud and Rothenflug, 1985), we have also estimated the theoretical period of slow modes at two other temperatures suitable for the inner corona. We find $P_{2nd\,slow} \approx 393$ s and 351 s, respectively, at temperatures $\log T_e = 6.0$ (1.0 MK), and $\log T_e = 6.1$ (1.25 MK). This way we find that our estimated periods do still remain in the close approximation of the observationally observed periods at these temperatures also. We measured the loop length simply using the difference image and assuming 10% uncertainty (Nakariakov and Ofman, 2001). The estimated loop-length may be a lower bound of the actual loop length. Hence, we examine our result assuming a range of uncertainties 10–30%. The theoretically estimated periods lie between 313 ± 31s and 313 ± 93 s. These periods do still remain in the close approximation of the observationally measured period. The 3-D stereoscopic reconstruction method for coronal loops as reported by Aschwanden et al. (1999b, 2002) measures the loop geometry more accurately. However, the analyses of the number of coronal loops using recent high-resolution space based observations, and such more advanced method to reconstruct the loop geometry, will be taken up in the future.

The second harmonic of the slow acoustic oscillations with a period ~322 s has a velocity node and pressure antinode at the loop apex. Therefore, it modifies the density leading to the intensity oscillations at the loop apex. Moreover, the second harmonic also has a velocity nodes and pressure anti-nodes at the footpoints. Hence, we expect that it will also modify the density much and show remarkable intensity oscillations at the footpoints. However, we did not observe the intensity oscillation with the power above the confidence level at the period around ~322 s (for example ~352 s at the location L_2) at the western footpoint. Therefore, the observed values are not exactly matching with the theory of second harmonics. The period of first harmonics dominates much at the footpoint. The theory of second spatial harmonics of slow acoustic oscillations [Eq. (2)] is given under the assumption of symmetric apex heating of the loops. Under such conditions, the density (and hence intensity) oscillatory power related with the second spatial harmonics of slow acoustic oscillations will peak at the loop apex (Tsiklauri et al., 2004; Nakariakov et al., 2004), while it will decrease as we move spatially towards the loop footpoints. Hence, the period of second harmonics shows the intensity variations by ~12% at the loop apex, while it might decreases below the 5% at the footpoint. Hence, probably we do not observe the dominant and statistically significant period of second harmonics at the western footpoint, which could not dominate over the first harmonics there (see Fig. 4: A closer peak of ~352 s to the second harmonics appeared at location L_2, which is not a well dominant oscillation period compared to the first harmonics of ~592 s).

We obtain two periods ~497 s and ~592 s for the western footpoint at locations L_1 and L_2, respectively, either of which may likely

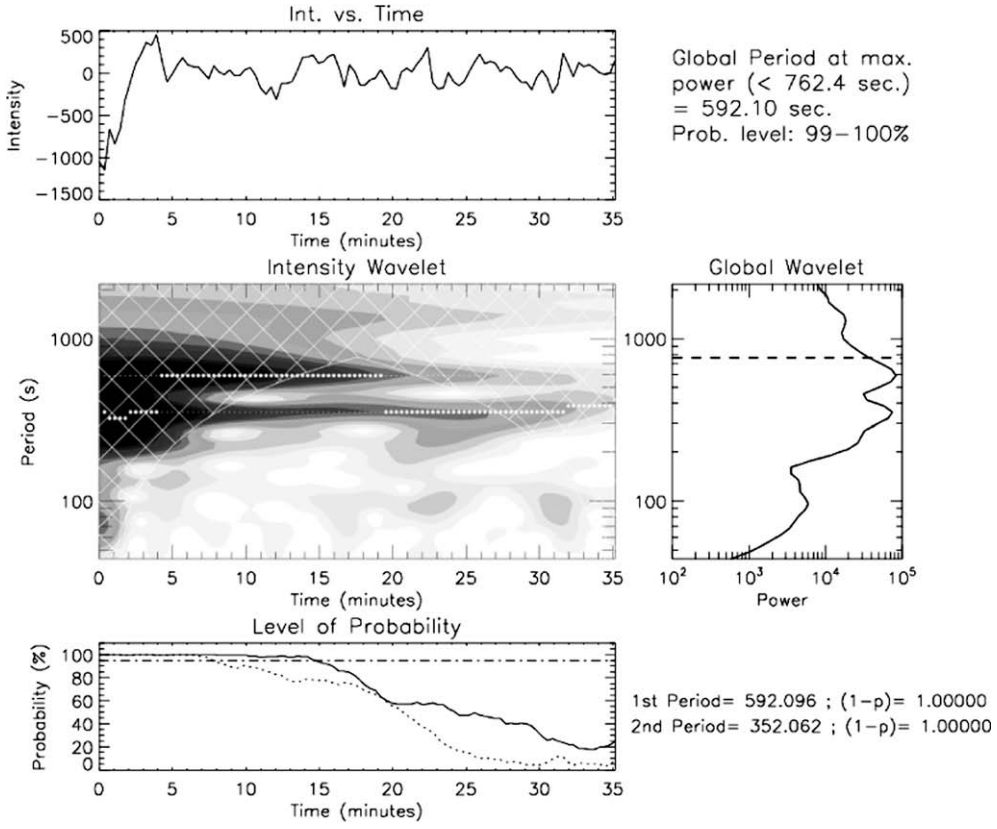

Fig. 4. The wavelet result for time series of Fe XII 195.12 Å: Top panel shows the variation of intensity, the wavelet power spectrum is given in the middle panel, and probability in the bottom panel. The light curve is extracted from L_2 location $(X_\lambda, Y_{SLOT}) \sim$ (32th pixel, 103th pixel) near the western footpoint.

be associated with the first harmonics (or fundamental mode) of the slow acoustic oscillations at the loop footpoint. Such mode has a velocity antinode and pressure node at the loop apex. Therefore, it neither modifies the density, nor shows any remarkable intensity oscillations at the loop apex. However, the first harmonic has velocity nodes and pressure anti-nodes at the footpoints. Hence, it modifies the density and causes remarkable intensity oscillations at the footpoint. It also modifies the density and can show intensity oscillations up to some extent above the footpoints. We locate the western footpoint of the selected loop in the diffused EUV loop system at two most probable locations L_1 and L_2. Accordingly, these two independent measurements of intensity oscillations at the locations L_1 and L_2 for the western footpoint with the periods of 497 s and 592 s, respectively, do not show correlation. Hence, both the independent observations at locations (L_1 and L_2) may likely be associated with the first harmonic of slow acoustic oscillations at the western footpoint. We further made the estimation of density scale heights using period ratio (P_1/P_2) of the observed period at apex to these two independently observed periods for the western footpoint.

The advantage of the wavelet analysis is that it shows the evolution of the oscillatory powers associated with the various periods in the 2-D (Fourier Period – Time) intensity wavelet. The global power spectrum is the time averaged power spectrum over the whole time series. The wavelet analysis of the apex (L_3 location) shows the enhanced and globally distributed power at statistically significant period of ~322 s. At the locations L_1, and L_2 near the western footpoint, the enhanced and globally distributed powers are at statistically significant periods of ~497 s and ~592 s, respectively. It should be noted that these periods are dominant, globally distributed, and statistically significant periods in the observational base-line of the this EUV loop by EIS/Hinode. The observations of such periodicities, respectively, near the loop apex and loop footpoint approximately match the theory as already noted. However, other periods may also be present in the power spectrum. These periods may not be statistically significant, or globally distributed, or both, at particular locations in the loop. For example, the period ~352 s at the L_2 location near western footpoint may also be considered as a signature of second harmonics of slow acoustic oscillations as it is very close to the observed period ~322 s near the apex. However, the ~352 s period shows ~1 cycle repetition over the total life span of the oscillation, while it might be able to repeat more than 4 cycles over the total time span of the observation to being statistically significant. Hence, this cannot be considered as a statistically significant period according to O'Shea and Doyle (2009).

The ratio between the periods of the first harmonics (or fundamental mode) and the second harmonics of the slow waves is proportional to $P_1/P_2 \sim 1.54$ (for the $P_1 = 322$ s, and $P_2 = 497$ s) and 1.84 (for the $P_1 = 322$ s, and $P_2 = 592$ s), which is significantly shifted from 2. Therefore, we find the first observational evidence of the period ratio shift of slow acoustic oscillations in the coronal loops. Similar phenomena were already observed for fast kink oscillations (Verwichte et al., 2004; De Moortel and Brady, 2007; Van Doorsselaere et al., 2007), and for sausage oscillations (Srivastava et al., 2008a) in the solar loops. The deviation of P_1/P_2 from 2.0 in homogeneous loops may be very small due to the wave dispersion (McEwan et al., 2006), however, longitudinal density stratification may cause significant shift of P_1/P_2 from 2.0 (Andries et al., 2005; McEwan et al., 2006; Van Doorsselaere et al., 2007). Using Eq. (24) of McEwan et al. (2006), period ratios $P_1/P_2 \sim 1.54$, 1.84 and half loop length $L_{1/2} \sim 33$ Mm, we estimate the density scale heights ~ 10 Mm and ~ 21 Mm in the coronal loop. This significant shift of period ratio from 2.0 is valid for the

longer loops where the density scale height is much lower compared to the loop half length (i.e., $L_{1/2} \ll \Lambda_c$) similar to our selected EUV loop.

It must be mentioned that seismologically estimated scale heights (depending upon two observed period ratios) 10 Mm, and 21 Mm in the coronal loop of half length $L_{1/2} \sim 33$ Mm, using the theory of McEwan et al. (2006), are smaller compared to the hydrostatical scale height, i.e., ~ 80 Mm at inner coronal temperature. It should also be noted that the scale height of ~21 Mm derived from the period ratio 1.84 (less shifted from 2.0) is more consistent and closer to the loop half length, while the height ~10 Mm derived from the period ratio 1.54 (more shifted from 2.0) is less compared to the loop half length. For the period of ratio 1.84 and density scale height of ~21 Mm, the intensity scale height is ~11 Mm. This means that the intensity at the apex is about 1/20 of the loop footpoints, which is inconsistent with the observations (cf., Fig. 5) and the loop apex should not be visible with this scale height. The same fact is also true for the period ratio 1.54 and thus the estimated density scale height ~10 Mm. However, the loop system shown in Fig. 5 indicates that the scale heights seem to be comparable to the loop length. Hence, the application of seismology based on McEwan et al. (2006) theory fails in this case. This may be simply because the assumption of hydrostatic loops is not realistic in the corona, or the loop studied in this case may not be hydrostatic.

The shift of period ratios may also be attributed to some other mechanisms (e.g., the variation of loop cross section with height). Recently, Verth and Erdélyi (2008) have studied the effect of magnetic stratification on loop transverse kink oscillations and found that the loop divergence may also have the significant effect on the period ratio almost similar to the density stratification. Since the slow wave is longitudinal compressive wave and weakly depends on the magnetic field in a plasma of low-beta, the magnetic stratification should not have a strong effect on the period of slow waves which is mainly affected by the temperature structure along the loop.

Our observational results also provide an evidence for the existence of impulsive heating localised in the solar corona for non-flaring cooler loops, complementing such evidences already discussed in the hot and flaring loops (e.g., Taroyan and Bradshaw, 2008; Nakariakov et al., 2004; Tsiklauri et al., 2004). However, we do not study the causes of localized impulsive heating. This will be taken up in our future works when we analyse various types of loops, both flaring and non-flaring existing at various temperatures.

One another interesting feature of these observations is the propagation/shifting of bright blob from west to east. From the temporal images (Fig. 5), we measure the travelled distance of the head of bright blob which is equal to ≈13,400 km. The time elapsed in this travel is 2100 s. Hence, the speed of the blob is ≈6.4 km/s, which is sub-sonic at coronal temperature ($T \sim 1.58$ MK). However, it should be noted that the approximately estimated propagation speed must be a lower bound of the actual sub-sonic speed of propagation, and the speed may be larger than the value reported here. It should also be noted that the blob becomes less brighter in the last two frames of the time sequence. At first instance, this indicates that this bright blob moves with the slow acoustic waves, and may be caused by such waves. However, the phase speed of slow waves is very close to the sound speed in a coronal loop, which should be 190 km/s at $T = 1.58\ MK$. De Moortel et al. (2002) measured the propagating speed of slow waves in the range 70–230 km/s in TRACE 171 Å. Therefore the speed of ~6 km/s is much less than the expected values. Hence, this could be caused by the heating or cooling of the loop. This bright blob is simply moving from one end to the other, but may not be a periodic feature. This is most likely a pulse of plasma flow in the coronal loop. Hence, the simultaneous presence of standing slow acoustic harmonics, and moving blob is very likely. However, more exact information about the bright blobs should be investigated using the high resolution images and spectral data.

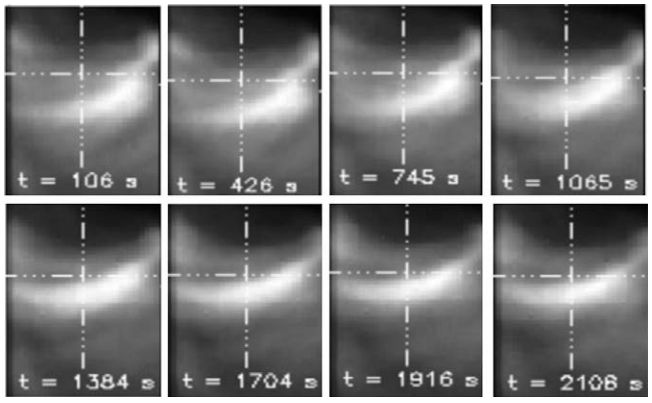

Fig. 5. The time sequence of the bright blob in the coronal loop.

Wang et al. (2005) have found the evidence of propagating 'blobs' of plasma in hot and flaring loops as seen by SUMER/SoHO. O'Shea et al. (2007) have also found simultaneous presence of propagating disturbances (PDs) and the harmonics of fast kink oscillations in TR loops cooled after flare. Mendoza-Briceño and Erdélyi (2006) have suggested the simultaneous presence of the standing oscillations, propagating waves, and moving 'cool gas blobs' in the loops. It should be noted that all these events are associated with the flaring loops and impulsive energy release, which can cause the complex dynamics in such loops. In this investigation, we find the propagating sub-sonic bright blob and multiple harmonic of acoustic oscillation, which is unique in the sense that the loop is non-flaring. This bright blob probably has no relation with the PDs of O'Shea et al. (2007) or with the hottest plasma blobs of Wang et al. (2005). The co-existence of sub-sonic blob is probably caused by mass flow from one end to other, and multiple acoustic harmonic in the non-flaring coronal loop formed around 1.58 MK. Therefore, this may shed new light on their evolution/excitation mechanisms.

Thermal conduction is suggested as an efficient dissipation mechanism for slow acoustic oscillations in hot and flaring loops (>6.0 MK) (Ofman and Wang, 2002; De Moortel and Hood, 2003). Sigalotti et al. (2007) have shown the importance of compressive viscosity as well as thermal conduction for damping the slow acoustic oscillations in hot coronal loops (>6.0 MK). However, Bogdan (2006) has found that mode conversion between acoustic and thermal modes causes the quick damping of the acoustic waves in the loops having apex pressure below a critical value. However, most of the coronal loops may have the apex gas pressure above critical pressure, hence the mode conversion cannot be possible. This makes thermal conduction damping mechanism inefficient. However, many previous findings show that the observed oscillations should also strongly decay within 3–4 cycles due to thermal conductive dissipation, which is an efficient dissipation mechanism. The intensity oscillation arising from the variation in plasma density (Fig. 2, top panel), does not show the signature of any dissipation within ~3 cycles when the ~322 s periodicity dominates in the time series. The similar observation has been noticed for the period ~497 s in the time-series from near the western footpoint. Hence, there should be more extensive investigations on the physical characteristics of damping mechanism for slow oscillations in comparatively cooler and non-flaring loops. The exact explanations are still open.

5. Discussion and conclusions

In this paper, we report for the first time, the observation of the multiple harmonics of slow acoustic oscillations in the non-flaring EUV loop. Such oscillations have been observed in the past, but only in hot and flaring coronal loops (Wang et al., 2002, 2005). While observations are rich for propagating acoustic waves, the lack of observational evidence for second harmonics of standing acoustic oscillations in cooler loops was a puzzle. The excitation mechanisms for propagating and standing oscillations are entirely different. The sub-photospheric p-mode acoustic oscillations penetrate through the chromosphere and transition region and excite the propagating slow acoustic waves in EUV loops. The second harmonics of slow mode oscillations, however, can be excited by the impulsive energy release in coronal loops. The most probable reason for the observational difficulties was the lack of a spectrometer with the appropriate temperature discrimination, sufficient spatial resolution, and most importantly high enough cadence.

Using 1-D loop hydrodynamic model and EIS/Hinode synthetic spectra, the observing possibilities of such oscillations were recently explored by Taroyan and Bradshaw (2008) with prediction that slow acoustic oscillations should be observed with the imaging as well as spectral analysis of real EIS/Hinode data. For the excitation of propagating acoustic waves by sub-photospheric p-modes penetrating into the corona, Taroyan and Bradshaw (2008) have shown that propagating acoustic waves can also be driven by impulsive energy releases, localised near loop footpoints, at frequencies differing from the fundamental mode frequency. Using spectroscopic observations from EIS/Hinode 1″ slit, recently Erdélyi and Taroyan (2008) have reported the first observational signature of slow acoustic oscillations in the cooler non-flaring loops.

In conclusion, using temporal image data fromEIS/Hinode 40″ slot, we report the signature of the second harmonics ($\sim$322 s) of slow acoustic oscillations in non-flaring coronal loops. In addition, we also find the periodicities $\sim$497 s and $\sim$592 s with the probability 99–100% at the 'L_1' and 'L_2' locations, respectively, near the clearly visible western footpoint of the loop. We interpret that these oscillations may likely be associated with the first harmonics (fundamental mode) of slow acoustic oscillations. Using the period ratios $P_1/P_2 = 1.54, 1.84$, we estimate the density scale heights in the EUV loop as $\sim$10 Mm and 21 Mm, respectively, which is not in hydrostatic equilibrium. We also find the evidence of propagating blob at its lower bound speed of $\approx$6.4 km/s which may be due to the pulse of plasma flow. Our investigation further suggests the simultaneous co-existence of standing oscillations, propagating bright blobs, in comparatively cooler and non-flaring coronal loop. This important new finding now stands for its further analysis and scrutiny with the rich source high-resolution data which will be forthcoming from the Hinode spacecraft.

Acknowledgments

We wish to express our gratitude to both the referees for their constructive comments/suggestions which improved the manuscript considerably. AKS thanks Prof. Ram Sagar (Director, ARIES) for all the help, support and encouragements, and Dr. E. O'Shea for kindly providing 'Randomlet'. We also thank Dr. T.V. Zaqarashvili for his valuable suggestions. Wavelet software was kindly provided by C. Torrence and G. Compo, and is available at http://paos.colorado.edu/research/wavelets/. Hinode is a Japanese mission developed and launched by ISAS/JAXA, with NAOJ as domestic partner and NASA and STFC (UK) as international partners. It is operated by these agencies in co-operation with ESA and NSC (Norway).

References

Andries, J., Arregui, I., Goossens, M., 2005. ApJ 624, L57.
Arnaud, M., Rothenflug, R., 1985. A&AS 60, 425.
Aschwanden, M.J., 1987. Sol. Phys. 111, 113.
Aschwanden, M.J., Newmark, J.S., et al., 1999b. ApJ 515, 842.
Aschwanden, M.J., Fletcher, L., Schrijver, C.J., Alexander, D., 1999a. ApJ 520, 880.
Aschwanden, M.J., De Pontieu, B., Schrijver, C.J., Title, A.M., 2002. Sol. Phys. 206, 99.
Banerjee, D., O'Shea, E., Doyle, J.G., Goossens, M., 2001. A&A 371, 1137.
Bogdan, T.Z., 2006. ApJ 643, 532.
Culhane, J.L., Doschek, G.A., Watanabe, T., et al., 2006. SPIE 6266, 62660.
De Moortel, I., Brady, C.S., 2007. A&A 664, 1210.
De Moortel, I., Hood, A.W., 2003. A&A 408, 755.
De Moortel, I., Ireland, J., Walsh, R.W., 2000. A&A 355, L23.
De Moortel, I., Ireland, J., Walsh, R.W., et al., 2002. Sol. Phys. 209, 61.
Erdélyi, R., Taroyan, Y., 2008. A&A 489, L45.
Gupta, A.C., Srivastava, A.K., Witta, P.J., 2009. ApJ 690, 216.
King, D.B., Nakariakov, V.M., DeLuca, E.E., et al., 2003. A&A 404, L1.
Linnell Nemec, A.F., Nemec, J.M., 1985. AJ 90, 2317.
Mathioudakis, M., Bloomfield, D.S., Jess, D.B., Dhillon, V.S., Marsch, T.R., 2006. A&A 456, 323.
McEwan, M.P., Donnelly, G.R., Díaz, A.J., Roberts, B., 2006. A&A 460, 893.
Mendoza-Briceño, C.A., Erdélyi, R., 2006. ApJ 648, 722.
Nakariakov, V.M., Ofman, L., 2001. A&A 372, L53.
Nakariakov, V.M., Ofman, L., DeLuca, E.E., Roberts, B., Davila, J.M., 1999. Science 285, 862.
Nakariakov, V.M., Melnikov, V.F., Reznikova, V.M., 2003. A&A 412, L7.
Nakariakov, V.M., Tsiklauri, D., Kelly, A., Arber, T.D., Aschwanden, M.J., 2004. A&A 414, L25.
Ofman, L., Wang, T., 2002. ApJ 580, L85.
O'Shea, E., Doyle, J.G., 2009. A&A 494, 355.
O'Shea, E., Banerjee, D., Doyle, J.G., Fleck, B., Murtagh, F., 2001. A&A 368, 109.
O'Shea, E., Banerjee, D., Doyle, J.G., 2005. A&A 436, L43.
O'Shea, E., Srivastava, A.K., Doyle, J.G., Banerjee, D., 2007. A&A 473, L13.
Pandey, J.C., Srivastava, A.K., 2009. ApJL 697, L153.
Popescu, M.D., Banerjee, D., O'Shea, E., Doyle, J.G., Xia, L.D., 2005. A&A 442, 1087.
Robbrecht, E., Verwichte, E., Berghmans, D., et al., 2001. A&A 370, 591.
Roberts, B., Edwin, P.M., Benz, A.O., 1984. ApJ 279, 857.
Sakurai, T., Ichimoto, K., Raju, K.P., et al., 2002. Sol. Phys. 209, 265.
Sigalotti, L., Di, G., Mendoza-Briceno, C.A., Luna-Cardozo, M., 2007. Sol. Phys. 246, 187.
Srivastava, A.K., Zaqarashvili, T.V., Uddin, W., Dwivedi, B.N., Kumar, P., 2008a. MNRAS 388, 1899.
Srivastava, A.K., Kuridze, D., Zaqarashvili, T.V., Dwivedi, B.N., 2008b. A&A 481, L95.
Taroyan, Y., Bradshaw, J., 2008. A&A 481, 247.
Taroyan, Y., Erdélyi, R., Doyle, J.G., Bradshaw, S.J., 2005. A&A 438, 713.
Torrence, C., Compo, G.P., 1998. BAMS 79, 61.
Tsiklauri, D., Nakariakov, V.M., Arber, T.D., Aschwanden, M.J., 2004. A&A 422, 351.
Ugarte-Urra, I., Doyle, J.G., Madjarska, M.S., O'Shea, E., 2004. A&A 418, 313.
Van Doorsselaere, T., Nakariakov, V.M., Verwichte, E., 2007. A&A 473, 959.
Verth, G., Erdélyi, R., 2008. A&A 486, 1015.
Verwichte, E., Nakariakov, V.M., Ofman, L., DeLuca, E.E., 2004. Sol. Phys. 223, 77.
Wang, T., Solanki, S.K., Curdt, W., Innes, D.E., Dammasch, I.E., 2002. ApJ 574, L101.
Wang, T.J., Solanki, S.K., 2004. A&A 421, L33.
Wang, T.J., Solanki, S.K., Innes, D.E., Curdt, W., 2005. A&A 435, 753.
Young, P.R., Del Zanna, G., Mason, H.E., Doschek, G.A., Culhane, J.L., Hara, H., 2007. PASJ 59, 857.